DOI: 10.1002/adma.200800052

X-Ray Induced Synthesis of 8H Diamond**

By *Zhongwu Wang,* Yusheng Zhao, Chang-sheng Zha, Qing Xue, Robert T. Downs, Ren-Guan Duan, Razvan Caracas,* and *Xiaozhou Liao*

The polymorphism of carbon is one of the striking features of its chemistry and physics, and its vapor, liquid, and solid polymorphs span a wide range of densities, bonding types, and physical and chemical properties. Consequently, there has been a long-standing interest in exploring the possible diamond polytypes. Since the hexagonal form (2H diamond or lonsdaleite) was found in meteorites,[1] evidence for other non-cubic polytypes has been reported.[2] Subsequent chemical vapor deposition (CVD) diamond studies have led to the observation of additional polytypes, including 4H, 6H, 8H, and 15R.[3–10] In these materials, particle size fractions range from 1000 nm down to 10 nm, and the phases are always mixed (e.g., 2H, 6H, 8H, and 3C). Recently, carbon nanotubes have been compressed to over 100 GPa, creating a single hard hexagonal phase dominated by sp^3-bonding.[11] The stability of the new phase at ambient conditions suggests potential applications. It appears that either modifying the morphology or decreasing the particle size, or a combination of both, can result in dramatically influencing the structural stability of carbon phases. Whether the goal is to make novel quenchable carbon polymorphs or to understand the transformational mechanisms, it is important to explore effective synthetic approaches.

Here, we report that samples of predominantly 8H diamond polytype can be synthesized at ambient pressure by intense 20 kW synchrotron X-ray radiation at the CHESS (Cornell High Energy Synchrotron Source) wiggler beam line.[12] Low-magnification Transmission Electron Microscopy (TEM) images reveal that the X-ray-induced carbon displays a particular lamellar morphology, and selected area electron diffraction (SAED) patterns display 12 symmetrical diffraction spots with *d*-spacings that range from 1.99 to 2.14 Å (Fig. 1). Two sets of diffraction spots were observed, and could be indexed as the same phase. Both the lamellar morphology and electron diffraction spots confirm the existence of an ordered twin structure with a twinning angle of 30° about a 3-fold axis of symmetry. This implies that the electron diffraction image is taken along either the [111] zone of cubic symmetry or the [001] zone of hexagonal symmetry. If the new phase was cubic diamond, then the innermost diffraction ring would correspond to (220) with a *d*-spacing of 1.54 Å. This peak is not observed in the experimental diffraction patterns, and therefore excludes the possibility that 3C diamond was synthesized. In addition, several diffraction peaks exist that can not be assigned to a cell for graphite, suggesting that the synthesis product is some other hexagonal polymorph of carbon. The lamellar habit of the synthesis product appears to be a consequence of a 90° twin rotation of adjacent layers stacked parallel to the hexagonal *c*-axis. The innermost ring of the diffraction pattern corresponds to (100) with a *d*-spacing of 2.14 Å. The four intense diffraction spots observed in Figure 1b still remain unexplained.

Synchrotron X-ray diffraction measurements together with simulations of the patterns were used to confirm the hexagonal structure. As is well known, SiC has a rich phase diagram with a large number of polymorphs and polytypes.[13] The relationship of the diffraction pattern of the newly synthesized carbon phase to that of the other carbon polytypes is similar to that observed between the hexagonal 4H, 6H, and 8H polytypes of SiC, all with space group $P6_3mc$. The diffraction peaks of the new hexagonal carbon phase can be accounted for, and indexed, with a model of

[*] Dr. Z. W. Wang
Cornell High Energy Synchrotron Source (CHESS)
Cornell University
Ithaca, NY 14853 (USA)
E-mail: zw42@cornell.edu
Dr. Z. W. Wang, Dr. Y. S. Zhao, Dr. Q. Xue
Dr. R.-G. Duan
Los Alamos National Laboratory
Los Alamos, NM 87545 (USA)
Dr. C.-S. Zha, Dr. R. Caracas
Geophysical Laboratory
Carnegie Institution of Washington
Washington DC 20015 (USA)
Dr. Q. Xue
Intel Corporation
Chandler, AZ 85226 (USA)
Prof. R. T. Downs
Department of Geosciences
University of Arizona
Tucson, AZ 85721-0077 (USA)
Dr. R.-G. Duan
Applied Materials, In.
Sunnyvale, CA 94085 (USA)
Dr. R. Caracas
Laboratoire de Sciences de la Terre CNRS UMR5570
Ecole Normale Supérieure de Lyon
Université Claude
Bernard – Lyon 1
69364 Lyon cedex 07 (France)
Dr. X. Z. Liao
School of Aerospace, Mechanical and Mechatronic Engineering
The University of Sydney
Sydney, NSW 2006 (Australia)

[**] This research was supported by the Department of Energy through Los Alamos National Laboratory and CDAC center. CHESS is supported by the National Science Foundation and NIH-NIGMS via NSF grant DMR-0225180. Special thanks go to Ms. Morgan Fillips for editorial assistance. We appreciate the reading, discussion and comments of Russell Hemley at Geophysical laboratory, Sol Gruner, Quan Hao and Don Bilderback at Cornell University, and Qun Shen at Argonne National Laboratory.

ADVANCED MATERIALS

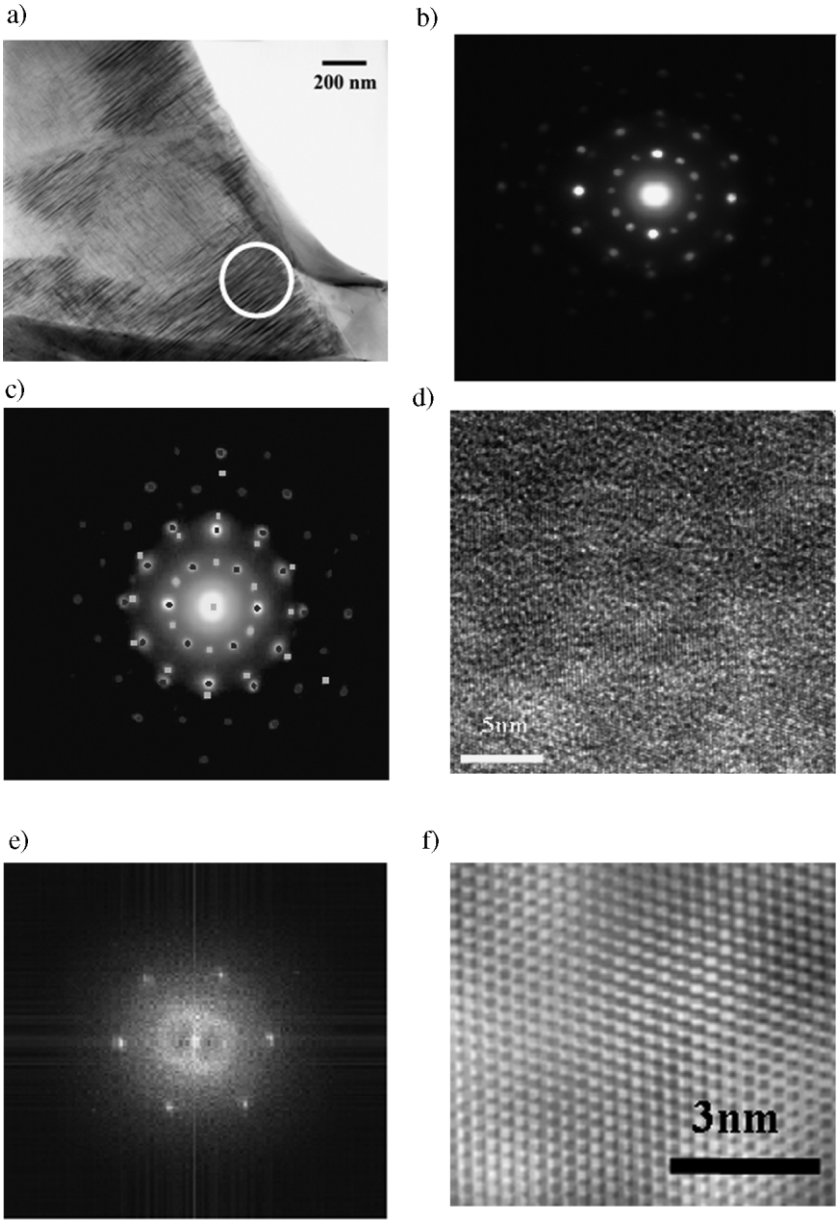

Figure 1. TEM images and electron diffractions of the X-ray induced carbon phase. a) low magnification twinning lamellar morphology; b) selected area electron diffraction Pattern (SAED) from the selected area in a; c) symmetry analysis of SAED, indicating that the two sets of electron diffraction spots, marked by black and white solid squares, respectively, are identical in structure; d) HRTEM image of a selected area; e) Fourier transformed SAED pattern; f) inverse transformed TEM image, showing the *d*-spacing of 2.05–2.14 Å.

the cell of one of the SiC polytypes in which the carbon atoms replace the silicon atoms, making the structure centrosymmetric.[13,14] Accordingly, the corresponding symmetries of these diamond polymorphs can be represented by space group $P6_3/mmc$ (#194; a supergroup of #186). We simulated the X-ray diffraction patterns of all possible structural candidates based on SiC polymorphs.[13,14] The simulated X-ray diffraction pattern of the 8H diamond polytype agrees in peak position and intensity with the observed diffraction pattern of the new phase. Each unit cell of 8H diamond consists of 16 carbon atoms stacked as 75% cubic diamond (3C) and 25% lonsdaleite (2H hexagonal diamond) (Fig. 2 and Table 1). There are 8 non-equivalent ways to make an eight layered closest packed sequence.[15] We found that the stacking sequence of the 8H diamond is *abcbacbc*, compared to *ab* in 2H lonsdaleite and *abc* in 3C diamond. This is the only eight layered stacking sequences that has a 75% cubic and 25% hexagonal component. The unit cell parameters are fully consistent with the electron diffraction data (Table 2). The calculated density of 3.67 g cm^{-3} (after the problems in the crystal structure table are resolved, then this density value might need to be recomputed) is similar to but greater than that of both cubic diamond and lonsdaleite (3.52 g cm^{-3}),[3,14] which suggests the existence of compressive stress, as discussed below. Both nanosized particles and compressive stress can produce broadening and slight shifts of the X-ray peaks consistent with the slight mismatch of some peaks in the observed and simulated patterns.

First-principles calculations were performed within the density-functional theory to examine the stability and properties of the 8H phase.[16–18] The results reveal that this phase is only about 3 meV/atom higher in energy than 3C diamond and significantly lower in energy (15 meV/atom) than 2H diamond. Both the relative energy differences as a function of volume (Fig. 3), along with the similar compressibilities of the 2H, 3C, and 8H phases (Table 3), are consistent with the superhardness expected for sp^3-bonded carbon. Indeed, the sp^3-bond character of 8H carbon, like that of 3C and 2H, is revealed by the calculated valence electron density distribution (Inset of Fig. 3) and by the electronic density of states (Fig. 4). 8H carbon not only combines the change distribution features of both the 2H and 3C diamond polymorphs in valence electron density distribution, but also displays very similar distributions of electron density of states to the 3C and 2H diamond polymorphs.

Symmetry group analysis indicates that the 8H structure has 16 Raman-active modes ($4A_{1g} + 4B_{1g} + 4E_{1g} + 4E_{2g}$), in which strong normal modes ($A_{1g} + B_{1g} + E_{1g}$) are expected to overlap in the frequency range of 1315 to 1350 cm^{-1}.[19–21] In 2H diamond, one strong peak corresponding to the A_{1g} mode is observed at 1325 cm^{-1},[22,23] whereas the frequency of the characteristic triply degenerate T_{2g} mode of 3C diamond is 1332 cm^{-1} (Fig. 5).[11,24] Based on the spectra of the synthesized 4H and 6H diamond and their mixtures with 3C

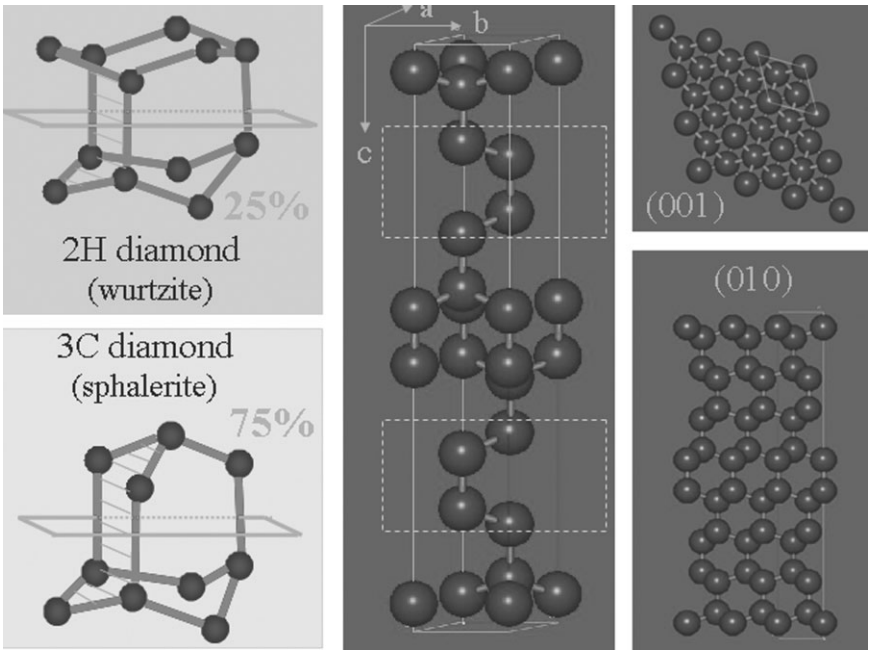

Figure 2. Crystallographic configurations of one unit cell of 8H diamond. Left: difference between cubic diamond (3C) with sphalerite structure and lonsdaleite (2H) with wurtzite structure. Middle) One unit cell of 8H diamond that includes 75% 3C diamond and 25% 2H diamond (marked by the dotted lines). Right: atomic arrangement of (001) and (010) facets of 8H diamond.

Table 1. Carbon atomic positions and cell parameters of 8H diamond structure.

Atomic Positions	Atomic number	*x*	*y*	*Z*[a]	*Z*[b]
4e	4	0	0	0.0469	0.0467
4f	4	0.3333	0.6667	0.0781	0.0779
4f	4	0.3333	0.6667	0.1719	0.1712
4f	4	0.3333	0.6667	0.7969	0.7974
a_0 [Å]	2.481(6)	Space group		$P6_3/mmc$	
c_0 [Å]	16.268(60)	Factor group		D_{6h}	
v_0 [Å^3]	86.8(5)	*Z*		16	

[a]Experimental. [b]Theoretical.

diamond,[4] the key Raman feature diagnostic of sp^3 carbon in 8H diamond is expected near ~1330 cm^{-1}; this feature is observed in the spectra of the 8H diamond (Fig. 5). Similar observations are reported for hexagonal-cubic diamond mixtures.[3] First-principles calculations are consistent with the present experiments, and indicate that the main broad peak is obtained by the superposition of E_{1g} (1304 cm^{-1}), B_{1g} (1322 cm^{-1}), A_{1g} (1332 cm^{-1}) and E_{2g} (1332 cm^{-1}) bands (Table 4). The experimental Raman band at 1581 cm^{-1} can be explained by residual graphite, partial sp^2 bonds, and surface dangling bonds (e.g., –C=C–). In this regard, we note that the material displays a twinned lamellar morphology with particle size or lamellar thickness of ~20 nm (Fig. 1A). This observation implies a high surface-to-volume ratio; dangling bonds expected to occur at the particle surface can lead to surface structure reconstruction to form C=C bonds. The short C=C bonds would introduce a compressive stress, giving rise to the higher density measured for 8H diamond relative to 3C diamond and lonsdaleite. Apparent surface reconstructions are observed in a large number of nanomaterials with compressive stress, and lead to a 3–7% volumetric contraction upon reducing the particle size from 100 nm to several nanometers,[25–27] consistent with the higher density of the 8H diamond compared to that of the 3C and 2H polymorphs.

An energetic high-temperature environment favors the nucleation of 3C and 2H diamond with a critical particle size of 2 nm, in which dislocations and stacking faults are not stable.[28] Rapid growth generates some stacking faults, and consequently results in the crystallization of other non-cubic

Table 2. Observed and calculated *d*-spacings of 8H diamond from electron and X-ray diffraction measurements, respectively.

H K L	Electron Diffraction[a]			X-ray Diffraction[b]			
	d-spacing [Å][c]	*d*-spacing [Å][d]	d_{obs}–d_{cal} [Å]	*d*-spacing [Å][c]	*d*-spacing [Å][d]	d_{obs}–d_{cal} [Å]	Intensity [%]
1 0 0	2.14	2.15	−0.01	2.163	2.151	0.012	8
1 0 1	2.11	2.13	−0.02	2.111	2.132	−0.021	25
1 0 2	2.08	2.08	0.00	2.073	2.079	−0.006	72
0 0 8	2.05	2.03	0.02	2.022	2.031	0.009	68
1 0 3	1.99	2.00	−0.01	2.001	1.999	0.002	100
1 0 4	1.91	1.90	0.01	1.911	1.901	0.010	7
1 0 10	–	–	–	1.293	1.296	−0.003	13
1 1 2	1.23	1.23	0.00	1.225	1.227	0.002	15
1 0 11	1.21	1.22	−0.01	–	–	–	
1 1 4	1.19	1.19	0.00	–	–	–	
1 0 12	1.15	1.15	0.00	1.148	1.146	0.002	7

[a]Using electron diffraction peaks, the cell parameter was calculated to be $a_0 = 2.48(1)$ Å, $c_0 = 16.27(6)$ Å and $V_0 = 86.8(5)$ Å^3. [b]Using X-ray diffraction peaks, the cell parameters were calculated to be $a_0 = 2.484(7)$ Å, $c_0 = 16.248(57)$ Å and $V_0 = 86.8(5)$ Å^3. [c]Observed. [d]Calculated.

ADVANCED MATERIALS

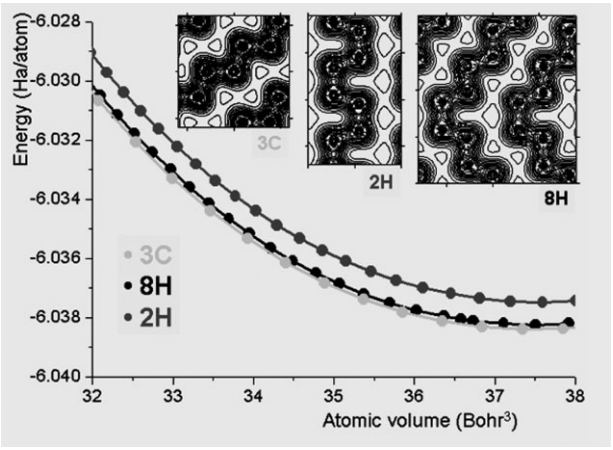

Figure 3. First-principles calculations of 8H compared with 3C and 2H diamond. As computed in the local density approximation of density functional theory, the energy differences as a function of volume between the three polymorphs 2H, 8H, and 3C are relatively similar. The volume is in bohr^3 (1 bohr = 0.529177 Å) and the energy in hartrees (1 Ha = 27.2116 eV). The inset shows cross-sections through the valence electron density. The charge distribution in 8H combines features from both the 2H and 3C polymorphs.

Table 3. Equation of state parameters for the three polymorphs 2H, 8H, and 3C from Vinet and 3rd order Birch–Murnagham (BM3) equations of states fitted on theoretical pressure – volume data.

Structure	Parameter	Vinet	BM3
3C	V_0 [bohr^3]	5.5546	5.5543
	K [GPa]	458	462
	K′[a]	6.505	3.590
2H	V_0 [bohr^3]	5.5705	5.5704
	K [GPa]	460	462
	K′[a]	6.450	3.621
8H	V_0 [bohr^3]	5.5577	5.5575
	K [GPa]	460	462
	K′[a]	6.435	3.616

[a]Unitless.

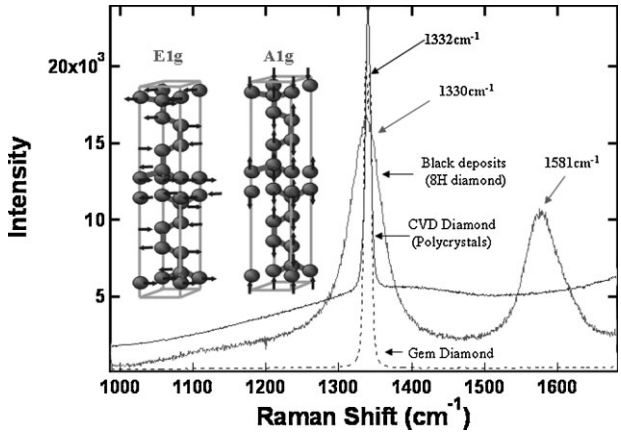

Figure 5. Raman spectra of diamond and synchrotron-formed black carbon powders. Insets show the displacement patterns for the dominant A_{1g} and E_{1g} Raman-active vibrational modes of 8H diamond.

Table 4. Frequencies of the Raman and infrared modes of 8H diamond computed using the density functional perturbation theory. The acoustic modes are $A_{2u} + E_{1u}$.

Raman modes [cm^{-1}]		Infrared modes [cm^{-1}]	
A_{1g}	732	A_{2u}	726
	1112		1276
	1332		1359
	1357		
B_{1g}	384	B_{2u}	389
	987		991
	1322		1311
	1360		1348
E_{1g}	405	E_{1u}	415
	546		1260
	1304		1299
	1353		
E_{2g}	236	E_{2u}	229
	519		508
	1265		1278
	1337		1335

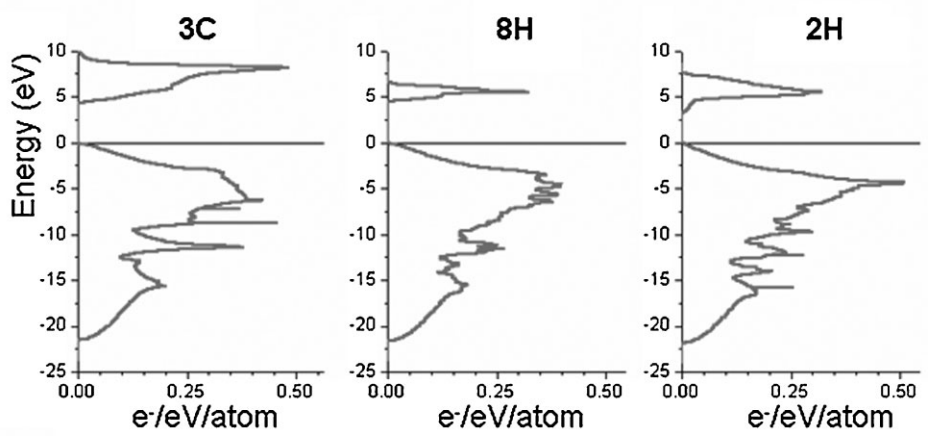

Figure 4. Electronic density of states (DOS) for the three polymorphs of diamond. The three distributions are similar, showing similar bonding of the sp^3 carbon in all three phases. The DOS is relative to the Fermi level.

hexagonal polymorphs, such as 8H diamond. Our experiments provide a similar energetic environment, in which the estimated temperature and pressure during photon pulse are about 4500 K and 10 GPa (8–15 GPa),[8,29–32] resulting in the formation of 8H diamond. These physical parameters certainly cast significant constraints for further simulations of new diamond polymorphs.[33] Due to the stability of 8H diamond at room conditions, the high density and stability of 8H diamond can provide new opportunities for making superhard materials with potential technolo-

gical applications.[34] In addition, X-ray radiation pervades the universe, but the shielding of harmful cosmic rays by the Earth's atmosphere and magnetic field may prevent the observation of natural radiation-induced processes at the Earth's surface. Thus, the discovery of X-ray induced synthesis of 8H diamond may also improve our understanding of planetary evolution, carbon stars, and interstellar dust.

Experimental

Synchrotron X-rays with a total power of 20 kW from the CHESS wiggler beamline were directed onto highly oriented pyrolytic graphite (HOPG) [12,29]. An adsorbed power of greater than 3 kW resulted in melting and evaporation of HOPG. Graphite is a low-Z element with excellent absorption of low energy X-ray. It is in the synchrotron orbit, but does not affect the experimental measurements using hard X-ray. About two months in one whole running circle have been used to collect sufficient samples for a series of additional analyses [8,29]. A sharp temperature gradient produced by the brazed water-cooling copper gasket led to a rapid deposition of the newly formed black carbon powders.

Transmission electron microscopy (TEM) investigations were carried out using a Philips CM 30 microscope operated at 300 kV, and high resolution TEM investigations were performed with a JEOL 3000F microscope operated at 300 kV. Electron diffraction using a 20 nm stationary probe yielded a convergent beam electron diffraction pattern at selected areas of the samples.

Energy dispersive X-ray diffraction measurements were performed at the Cornell High-Energy Synchrotron Source (CHESS)[12,29]. The samples were removed to fill a sample chamber for x-ray diffraction measurement. The small chamber was made by a stainlessness gasket includes a drilled hole with a diameter of 250 μm and thickness of 70 μm. The beam size was collimated down to 40 μm. Energy calibrations were made by using the well-known radiation sources of ^{55}Fe and ^{133}Ba, and angle calibrations were made at a fixed angle of 11° from the five peaks of standard Au powder. X-ray diffraction pattern at each sample spot was collected for 24 h.

Both the commercial crystallographic software and Rietveld refinement program (Jade and *GSAS*) were employed to simulate X-ray diffraction spectra of different carbon polymorphs transformed from SiC polytypes. The atomic positions and unit cell parameters obtained from electron and synchrotron X-ray diffraction were used to synthesize the diffraction patterns. The resulting patterns were converted from 2Θ (°) to energy (keV) for comparison.

We perform first-principles calculations using the local density approximation (LDA) of density functional theory in the ABINIT implementation, based on plane waves and pseudopotentials [16]. Upon use of the Troullier–Martins scheme for pseudopotentials [17], we sample the electron density in the reciprocal space in the first Brillouin zone using a grid of special high-symmetry **k** points. As usual in the plane wave–pseudopotential implementations the accuracy of the calculations can be improved by raising the number of plane waves through increasing the threshold on their kinetic energy and by densifying the sampling of the Brillouin zone. Meanwhile, we adopt a 40 hartree (1 hartree = 27.2116 eV) kinetic energy cutoff that ensures a convergence in total energy better than 1 mHa and in pressure better than 1 GPa, and also use the density functional perturbation theory to determine the dielectric and the lattice dynamical properties [18].

Raman spectra were excited with a green laser tuned to a wavelength of 532.15 nm, and transported by an optical fiber with a diameter of 5 μm, and thus collected through an 1800 grating monochrometer/spectrograph (resolution 2 cm^{-1}) to an electronic-cooled charge-coupled device detector. The laser beam was focused through a microscope, and the beam with a low power of 2 mW was used to avoid heating the sample.

Received: January 7, 2008
Revised: March 17, 2008
Published online:

[1] R. E. Hanneman, H. M. Strong, F. P. Bundy, *Science* **1967**, *155*, 995.
[2] R. Kapil, B. R. Mehta, V. D. Vankar, *Thin Solid Films* **1998**, *312*, 106.
[3] P. D. Ownby, X. Yang, J. Liu, *J. Am. Ceram. Soc.* **1992**, *75*, 1876.
[4] S. Bhargava, H. D. Bist, S. Sahli, M. Aslam, H. B. Tripathi, *Appl. Phys. Lett.* **1990**, *67*, 1706.
[5] L. C. Chen, T. Y. Wang, J. R. Yang, K. H. Chen, D. M. Bhusari, Y. K. Chang, H. H. Hsieh, W. F. Pong, *Diamond Relat. Mater.* **2000**, *9*, 877.
[6] O. G. Epanchintsev, *J. Phys. Chem. Solids* **1997**, *58*, 1243.
[7] D. M. Gruen, S. Z. Liu, A. R. Krauss, J. S. Luo, X. Z. Pan, *Appl. Phys. Lett.* **1994**, *64*, 1502.
[8] F. P. Bundy, *Phys. A* **1989**, *156*, 695.
[9] A. Laikhtman, I. Gouzman, A. Hoffman, *Diamond Relat. Mater.* **2000**, *9*, 1026.
[10] M. Rossi, G. Vitali, M. L. Terranova, V. Sessa, *Appl. Phys. Lett.* **1993**, *63*, 2765.
[11] Z. W. Wang, Y. S. Zhao, K. Tait, X. Z. Liao, D. Schiferl, C. S. Zha, R. T. Downs, J. Qian, Y. T. Zhu, T. D. Shen, *Proc. Natl. Acad. Sci. USA* **2004**, *101*, 13699.
[12] Z. W. Wang, L. L. Daemen, Y. S. Zhao, C. S. Zha, R. T. Downs, X. D. Wang, Z. L. Wang, R. J. Hemley, *Nat. Mater.* **2005**, *4*, 922.
[13] P. T. B. Shaffer, *Acta Crystallogr.* **1969**, *25*, 477.
[14] A. W. Phelps, W. Howard, D. K. Smith, *J. Mater. Res.* **1993**, *8*, 2835.
[15] R. M. Thompson, R. T. Downs, *Acta Crystallogr. Sect. B* **2001**, *57*, 766.
[16] X. Gonze, J. M. Beuken, R. Caracas, F. Detraux, M. Fuchs, G. M. Rignanese, L. Sindic, M. Verstraete, G. Zerah, F. Jollet, M. Torrent, A. Roy, M. Mikami, P. Ghosez, J. Y. Raty, D. C. Allan, *Comput. Mater. Sci.* **2002**, *25*, 478.
[17] N. Troullier, J. L. Martins, *Phys. Rev. B* **1991**, *43*, 1993.
[18] X. Gonze, G.-M. Rignanese, R. Caracas, *Z. Kristallogr.* **2005**, *220*, 458.
[19] D. W. Feldman, J. H. Parker, W. J. Choyke, L. Patrick, *Phys. Rev.* **1968**, *173*, 787.
[20] S. Nakashima, H. Katahama, Y. Nakakura, A. Mitsuishi, *Phys. Rev. B* **1986**, *33*, 5721.
[21] K. E. Spear, A. W. Phelps, W. B. White, *J. Mater. Res.* **1990**, *5*, 2277.
[22] H. K. He, T. Sekine, T. Kobayashi, *Appl. Phys. Lett.* **2002**, *81*, 610.
[23] B. R. Wu, J. Xu, *Phys. Rev. B* **1998**, *57*, 13355.
[24] M. Yoshikawa, Y. Mori, M. Maegawa, G. Katagiri, H. Ishida, A. Ishitani, *Appl. Phys. Lett.* **1993**, *62*, 3114.
[25] C. B. Duke, *Chem. Rev.* **1996**, *96*, 1237.
[26] A. Puzder, A. J. Williamson, F. Gygi, G. Galli, *Phys. Rev. Lett.* **2004**, *92*, 217401.
[27] Z. W. Wang, K. Tait, Y. S. Zhao, C. S. Zha, H. Uchida, R. T. Downs, *J. Phys. Chem. B* **2004**, *108*, 11506.
[28] a) M. A. Meyers, A. Mishra, D. J. Benson, *Prog. Mater. Sci.* **2006**, *51*, 427. b) Z. W. Wang, K. Finkelstein, C. Ma, Z. L. Wang, *Appl. Phys. Lett.* **2007**, *90*, 113115. c) Z. W. Wang, S. Seal, S. Patil, C. S. Zha, Q. Xue, *J. Phys. Chem. C* **2007**, *111*, 11756.
[29] B. W. Batterman, N. W. Ashcroft, *Science* **1979**, *206*, 157.
[30] A. Sorkin, J. Adler, R. Kalish, *Phys. Rev. B* **2006**, *74*, 064115.
[31] Z. W. Wang, P. Lazor, S. K. Saxena, *Phys. B* **2001**, *293*, 408.
[32] S. E. Hardcastle, H. Zabel, *Phys. Rev. B* **1983**, *27*, 6363.
[33] S. Reich, C. Thomsen, *Phys. Rev. B* **2002**, *65*, 153407.
[34] H. W. Kroto, J. R. Heath, S. C. Obrien, R. F. Curl, R. E. Smalley, *Nature* **1985**, *318*, 162.

